Margination of Micro- and Nano-Particles in Blood Flow and its Effect on the Efficiency of Drug Delivery

Kathrin MÜLLER[1], Dmitry A. FEDOSOV[1*], Gerhard GOMPPER[1]

1: Theoretical Soft Matter and Biophysics, Institute of Complex Systems and Institute for Advanced Simulation, Forschungszentrum Jülich, 52425 Jülich, Germany
* Corresponding author: Tel.: +49 (0)2461 612972; Fax: +49 (0)2461 613180; Email: d.fedosov@fz-juelich.de

Abstract Drug delivery by various micro- and nano-carriers offers the possibility of controlled transport of pharmaceuticals to targeted sites (e.g., cancerous tissue). Even though the fabrication of carriers of different sizes and shapes with a number of functionalities has made much progress in the last decade, their delivery including controlled particle distribution and adhesion within the body remains a great challenge. The adhesion of micro- and nano-carriers in blood flow is strongly affected by their distribution within the vessel cross-section. To investigate the adhesion potential of carriers of different shapes and sizes, we employ mesoscopic hydrodynamic simulations of blood flow in order to predict margination of carriers or their migration properties toward vessel walls. The margination of carriers is studied for a wide range of hematocrit values, and flow rates, using a two-dimensional blood-flow model. Two different particle shapes (spherical and ellipsoidal) and various sizes, ranging from about hundred nanometers to several micrometers, are considered. We find that the margination properties of particles worsen with decreasing carrier size. Spherical particles yield slightly better margination than ellipsoidal particles; however, adhesion of ellipsoidal carriers is expected to be superior due to a larger area for adhesive interactions. As a conclusion, micron-size ellipsoidal particles seem to be favorable for drug delivery in comparison to sub-micron particles and spherically shaped carriers.

Keywords: Red Blood Cell, Drug Carrier, Flow Migration, Margination Probability, Particle Distribution, Dissipative Particle Dynamics

1 Introduction

The use of micro- and nano-carriers for targeted drug delivery provides promising strategies for the treatment of various diseases such as cancer (Ferrari, 2005; Jain and Stylianopoulos, 2010). However, design and physical delivery of the particles carrying different contrast agents and drugs are very challenging tasks. Several important aspects in the fabrication process have to be taken into account, including bio-compatibility, durability, binding to specific targets, and the ability of controlled release. Even though micro- and nano-particle fabrication has been strongly advanced in recent years (Duncan, 2006; Rolland et al., 2005; Davis et al., 2008; Blanco et al., 2011), the delivery of carriers to targeted sites is still poorly understood (Jain and Stylianopoulos, 2010; Sanhai et al., 2008; Huang et al., 2010). Determination of the distribution of micro- and nano-carriers in the organism following systemic administration has been named as one of the several challenges in nanomedicine (Sanhai et al., 2008). The other challenge for drug delivery is often called biological barriers (Jain, 1989), which include particle transport through microvascular walls, interstitial space, and cell membranes (Jain and Stylianopoulos, 2010; Sanhai et al., 2008).

The first step in the delivery of small carriers is their transport along blood vessels which determines their initial distribution. Further, the distribution of micro- and nano-particles is affected by their binding to specific targeted sites. However, efficient binding of carriers

can be achieved only if they are present near vessel walls at sufficiently high concentrations, and thus, the distribution of micro- and nano-carriers within vessel cross-sections plays an essential role in their efficient delivery. The cross-sectional distribution of micro- and nano-particles depends on local blood flow properties such as hematocrit (volume fraction of red blood cells) and flow rate as well as on the particle characteristics such as their size, shape, and deformability. The migration of various suspended particles toward walls in blood flow, which is also often referred to as *margination*, has been observed for white blood cells (Bagge and Karlsson, 1980; Goldsmith and Spain, 1984; Fedosov and Gompper, 2014), platelets (Tangelder et al., 1985; Woldhuis et al., 1992), and rigid micro-particles (Tilles and Eckstein, 1987; Eckstein et al., 1988). Particle margination in blood flow is mediated by red blood cells (RBCs), which migrate to the vessel center (Goldsmith et al., 1989) due to hydrodynamic interactions with the walls (called lift force) (Cantat and Misbah, 1999; Abkarian et al., 2002; Messlinger et al., 2009), and lead to an increased concentration of different particles within the RBC-free layer (RBCFL) near a wall (a layer void of RBCs). More precisely, the margination mechanism is a consequence of the competition between lift forces on RBCs and suspended particles, and their interactions in flow (Kumar and Graham, 2012). Similarly, micro- and nano-carriers have a potential to get marginated (Müller et al., 2014), and therefore to interact with vessel walls.

The role of particle size and shape in the efficient delivery is a multi-faceted problem. Large enough particles with a characteristic size greater than approximately 4 μm may get trapped in the smallest capillaries of the body (Slack et al., 1981). On the other hand, particles with a size of only a few nanometers are rapidly excreted through the kidneys (De Jong et al., 2008). Studies with intravascularly injected silica particles with a moderate size (from 700 nm to 3 μm) have shown that smaller particles yield a more uniform distribution in various organs in comparison with the larger ones (Decuzzi et al., 2010). In addition, an enhanced accumulation of the particles in the organs has been found for particles having a discoidal shape (Decuzzi et al., 2010). However, particle internalization by macrophages appears to be reduced for elongated particles (Champion and Mitragotri, 2006). Adhesion of different particles has been studied experimentally (Gentile et al., 2008) and theoretically (Decuzzi and Ferrari, 2006); these studies show that oblate ellipsoids are subject to stronger adhesion than spheres with the same volume. To better understand adhesive potential of micro- and nano-carriers, quantitative description of particle margination under realistic blood flow conditions is required.

Numerical simulations of blood flow on a single-cell level allow us to explore the flow behavior and interaction of blood cells and other suspended components (Fedosov et al., 2014b; Freund, 2014; Fedosov et al., 2014a). In this work, we investigate the role of particle size and shape on the margination efficiency, and therefore adhesion, since particle margination is an essential pre-condition for particle adhesion (Müller et al., 2014). Several sizes ranging from several microns to about one hundred nanometers and two different shapes (spherical and ellipsoidal) are considered. The margination of micro- and nano-particles is studied for a wide range of hematocrit values and flow rates using mainly two-dimensional (2D) simulations. Our findings show that spherical particles have slightly better margination properties than ellipsoids, however the adhesion efficiency of ellipsoidal particles appears to be superior in comparison with that of spheres due to a larger area for adhesive interactions (Decuzzi and Ferrari, 2006). The larger particles possess a larger probability of being marginated. As the particle size becomes very small (less than 100 – 200 nm), the particle distribution within vessel cross-section can be described well by the volume excess of flowing RBCs.

2 Models and methods

Simulation method. Our simulations are based on the dissipative particle dynamics (DPD) method (Hoogerbrugge and Koelman, 1992; Español and Warren, 1995), a mesoscopic particle-based approach which captures full hydrodynamics. The simulated system is represented by a collection of point particles which interact locally through three pairwise forces: a conservative, dissipative, and random force. The time evolution of the velocity and position of the particles is determined by the Newton's second law of motion.

Modeling cells and particles. RBCs in 2D are modeled as closed bead-spring chains of N_s connected particles, which incorporate bending rigidity and an area constraint (Fedosov et al., 2012). Suspended micro- and nano-carriers are represented by a collection of N_v^p particles, which are constrained to maintain a rigid configuration.

Simulation setup. The simulated system corresponds to a 2D channel with a width of $W = 20\,\mu\text{m}$. Figure 1 displays a simulation snapshot for a hematocrit (the area fraction of RBCs) of $H_t = 0.3$. The flow is confined by two walls which are modeled using frozen fluid particles in combination with a bounce-back reflection of flow particles at the fluid-wall interface (Fedosov and Karniadakis, 2009). In flow direction, periodic boundary conditions are assumed and blood flow is driven by a constant force applied to each solvent particle, which is equivalent to a prescribed pressure drop. In order to characterize the flow strength, we define a non-dimensional shear rate as

$$\dot{\gamma}^* = \bar{\dot{\gamma}}\tau_{RBC} = \bar{\dot{\gamma}}\frac{\eta D_r^3}{\kappa_r}, \qquad (1)$$

where $\bar{\dot{\gamma}} = \bar{v}/W$ is the average shear rate (or pseudo shear rate) and $\bar{v}$ is the average flow velocity, while τ_{RBC} defines a characteristic RBC relaxation time. Here, η is the solvent's dynamic viscosity, $D_r = L_0/\pi$ is the corresponding RBC diameter with L_0 being the cell contour length, and κ_r is the RBC membrane bending rigidity. The RBCs are further characterized by the reduced area $A^* = 4A_0/(\pi D_r^2) = 0.46$, where A_0 is the enclosed RBC area. Typical values for real healthy RBCs are $D_r = 6.1\,\mu\text{m}$, $\eta = 1.2 \times 10^{-3}\,\text{Pa s}$, and $\kappa_r = 50 k_B T$ for the physiological temperature $T = 37\,^\circ\text{C}$.

Measuring RBC-free-layer thickness. To determine the RBC-free-layer (RBCFL) thickness, we measure the outer edge of the RBC core, which is similar to RBCFL measurements in experiments (Maeda et al., 1996; Kim et al., 2007). The data is averaged for many RBC snapshots at different times.

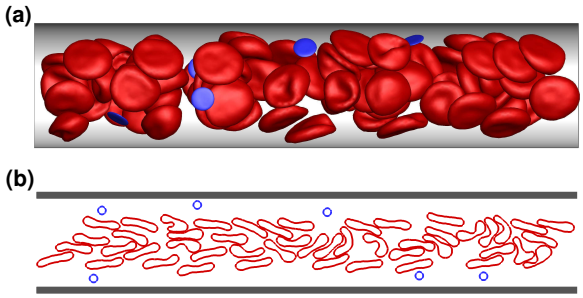

Figure 1: Snapshots of RBC and particle conformations in microchannels in 3D and 2D. RBCs are colored in red and suspended particles in blue. (a) 3D simulation snapshot of blood flow for $H_t = 0.3$ and $\dot{\gamma}^* \approx 39$. (b) 2D simulation snapshot of blood flow for $H_t = 0.3$ and $\dot{\gamma}^* \approx 29.3$.

3 Results

3.1 Carrier margination

Margination of micro- and nano-carriers in blood flow depends on hematocrit H_t and flow rate characterized by $\dot{\gamma}^*$ (Müller et al., 2014). Numerical simulations performed for different conditions allow us to measure the distributions of particles across the flow, which reflect the probability of a particle to be at a certain radial position. Figure 2 shows several center-of-mass distributions of circular particles with $D_p = 0.3 D_r$ ($D_p = 1.83\,\mu\text{m}$) for several H_t values and $\dot{\gamma}^* \approx 29.3$. The distributions have been averaged over the halves of the channel due to symmetry. The distributions indicate

that as H_t increases the carriers marginate better, since a strong peak in the distributions develops and its position moves closer to the wall at $y/W = 0$. This trend is in agreement with the margination of blood platelets, which have a comparable size, such that platelet margination has been observed to increase with increasing H_t in experiments (Tilles and Eckstein, 1987) and simulations (Crowl and Fogelson, 2011; Zhao and Shaqfeh, 2011; Reasor Jr et al., 2013). The distributions in Fig. 2 also show that the carriers migrate into the RBCFL near a wall and remain quasi-trapped there. The shift of the peak toward the wall is due to a decrease in the RBCFL thickness as H_t is increased, leading to a smaller available space for marginated particles.

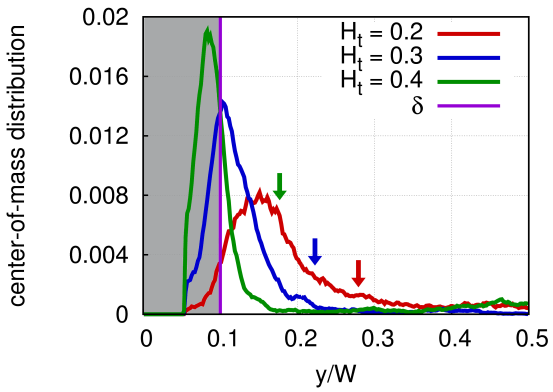

Figure 2: Particle distribution across the channel. Center-of-mass distribution of carriers for various H_t values at $\dot{\gamma}^* \approx 29.3$. 2D simulation results for circular particles with $D_p = 0.3D_r$ ($D_p = 1.83\,\mu$m). The wall is at $y/W = 0$. The shaded area indicates schematically a region with a thickness δ near the wall. The arrows indicate the boundary of the RBCFL for the different hematocrits, marked by corresponding colors.

To quantify particle margination we define the margination probability as a probability of a particle center-of-mass to be within a certain distance away from the wall. This is sketched in Fig. 2 with a selected distance of $\delta = 0.33D_r$ (about 2 µm), which is smaller than the RBCFL thickness in most cases. Other choices for the distance δ are possible and discussed by Müller et al. (2014). Figure 3 presents margination probability diagram of particles for a wide range of H_t values and non-dimensional shear rates. The aforementioned dependence of particle margination on H_t is observed essentially for every flow rate. Particle margination also shows a strong dependence on $\dot{\gamma}^*$, which is most pronounced at low shear rates. Simulated values of $\dot{\gamma}^*$ cover the range of flow rates characteristic for the venular part of microcirculation, where it is estimated that $\dot{\gamma}^* \lesssim 90$ in 3D ($\dot{\gamma}^* \lesssim 77$ in 2D), while in arteriolar part the flow rates are higher with $\dot{\gamma}^* \gtrsim 120$ in 3D (Popel and Johnson, 2005; Pries et al., 1995). This range of shear rates is also relevant for tumor microvasculature, since blood flow velocities in tumors are much reduced in comparison to those in normal microvasculature due to high geometric resistance and vessel permeability (Jain, 1988; Yuan et al., 1994).

The margination probability diagram in Fig. 3 shows that the strongest particle margination is found for the range of $H_t = 0.25 - 0.6$. This region has a considerable overlap with the characteristic hematocrits in the body's microvascular networks in the range $H_t = 0.2$–0.4. A strong particle margination at high H_t values seems to be an advantage for drug delivery to tumors, since blood within tumor microvasculature is often subject to hemo-concentration due to plasma leakage (Sevick and Jain, 1989).

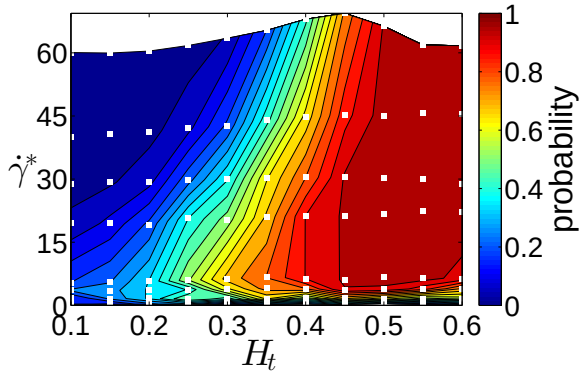

Figure 3: Particle margination diagram. Probability diagram of particle margination with respect to $\dot{\gamma}^*$ and H_t. The white squares indicate the values of H_t and $\dot{\gamma}^*$ for which simulations have been performed. The margination probabilities are calculated from the particle center-of-mass distributions using a distance of $\delta = 0.33D_r$ (2 µm) away from the wall.

3.2 Dependence of margination on particle size.

The discussion above considered the margination effect of micron-size particles, however there exists a strong interest in nano-carriers with sizes starting from several nanometers. Figures 4(a),(b) show the probability diagrams which characterize margination properties of particles with $D_p = 0.15D_r$ ($D_p = 0.91\,\mu$m) and $D_p = 0.04D_r$ ($D_p = 250\,$nm), respectively. Visual examination of Fig. 4(a),(b) and Fig. 3 for $D_p = 0.3D_r$ ($D_p = 1.83\,\mu$m) indicates that the region of high margination probability becomes smaller as the particle size is decreased. Thus, we can conclude that the margination of particles worsens as the carrier size becomes smaller, which is similar to the results found by Müller et al. (2014).

To illustrate the reason for the reduction in particle margination probability with decreasing particle size, we present in Fig. 4(c) the distributions of particles with different sizes across the channel for $H_t = 0.3$ and $\dot{\gamma}^* \approx 29.3$. For large enough particles we observe a pronounced peak in the distribution next to the wall due their interactions with RBCs leading to particle quasi-confinement within the RBCFL, since the particle size is comparable with the RBCFL thickness. Even though small particles are also subject to the margination effect, their distribution within the RBCFL is more uniform and their presence around the vessel centerline is slightly more probable than that for larger particles. Thus, the cumulative probability for a single particle to be within a layer of thickness $0.33D_r$ near the wall is lower for nano-carriers than that for micro-particles. An interesting observation, however, is that the distribution of the smallest simulated particles with $D_p = 0.04D_r$ ($D_p = 250\,$nm) closely approaches the distribution computed as the excess volume of flowing RBCs. This indicates that the distribution of particles smaller in size than approximately 250 nm can be well approximated by the blood plasma volume, and therefore their margination properties can be directly inferred from the local H_t distribution.

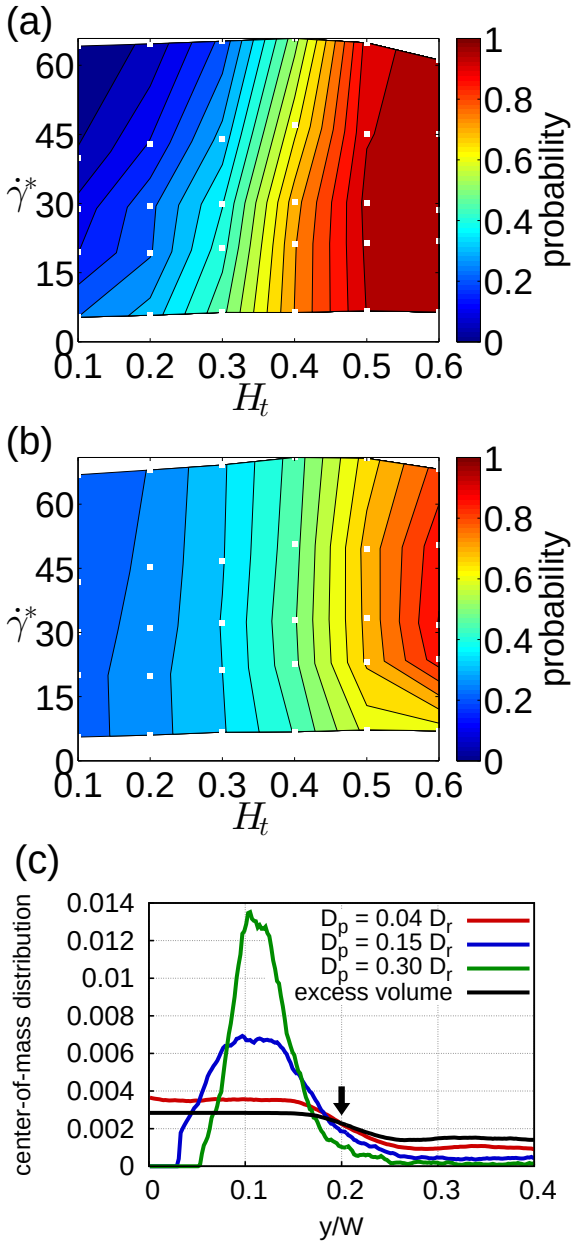

Figure 4: Dependence of margination on particle size. Probability diagrams of particle margination for various H_t and $\dot{\gamma}^*$ values and for circular particles with the sizes (a) $D_p = 0.15D_r$ ($D_p = 0.91\,\mu$m), (b) $D_p = 0.04D_r$ ($D_p = 0.25\,\mu$m). The white squares indicate the values of H_t and $\dot{\gamma}^*$ for which simulation were performed. The margination probability is calculated based on the distance of $0.33D_r$ ($2\,\mu$m) away from the wall. (c) Distribution of particles with different sizes across the channel for $H_t = 0.3$ and $\dot{\gamma}^* \approx 29.3$. For small particles the distribution resembles the curve computed as the excess RBC volume and drawn by black solid line. The arrow denotes position of the RBCFL boundary.

3.3 Dependence of margination on particle shape.

Advances in micro- and nano-particle fabrication allow the production of carriers in various shapes, including a sphere, ellipsoid, and a rod-like shapes (Rolland et al., 2005). However, advantages of different particle shapes for drug delivery are still not well explored. Recent theoretical (Decuzzi and Ferrari, 2006; Dasgupta et al., 2013) and experimental (Gentile et al., 2008) studies suggest that ellipsoidal particles possess better adhesion properties than spheres due to a larger area for adhesion interactions. To explore the effect of particle shape on the margination properties in blood flow, we performed a number of simulations with ellipse-shaped particles. Figure 5 shows the margination probability diagram for an ellipse-like particle under various blood flow conditions. The ellipse has an aspect ratio of about 7. The ellipse area corresponds to the area of a circle with the diameter $D_p = 0.22D_r$, so that the comparison of the margination diagram in Fig. 5 can be best made with those in Figs. 3 and 4(a). Visual inspection of the margination probability diagrams for spherical and ellipsoidal particles indicates that the corresponding diagrams are qualitatively similar. A quantitative analysis shows that the margination of ellipsoidal particles appears to be slightly less efficient than that of spheres; however, the differences are not very significant. Note that these findings also indicate that ellipsoidal particles with a smaller aspect ratio than 7 have margination properties similar to those presented in Figs. 3 and 5. In conclusion, the current knowledge about adhesion of ellipsoidal particles and our simulation results on margination suggest that ellipsoidal particles are likely to be a better choice for drug delivery.

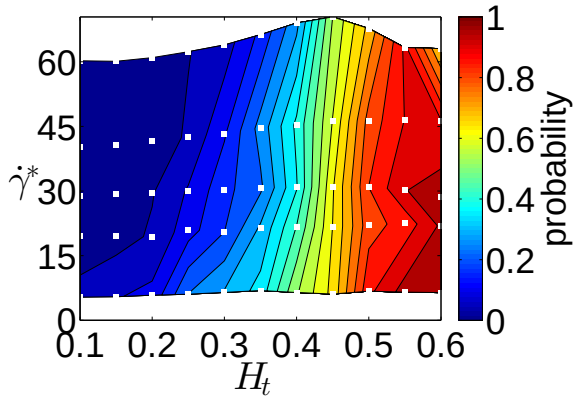

Figure 5: Dependence of margination on particle shape. Probability diagram of particle margination for various H_t and $\dot{\gamma}^*$ values and for the ellipse-like particles. The long axis of a 2D elliptic particle is $L_p = 0.63D_r$ (3.84 µm) and an aspect ratio is equal to approximately 7. The white squares indicate the values of H_t and $\dot{\gamma}^*$ for which simulation were performed. The margination probability is calculated based on the distance of $0.33D_r$ away from the wall.

4 Summary

In summary, particle margination in blood flow strongly depends on particle size and shape, hematocrit, and flow rate. Margination of both spherical and ellipsoidal particles increases with increasing hematocrit, while their margination properties appear to be rather similar, where a sphere marginates slightly more efficiently than an ellipsoid. The presented diagrams show that larger particles have a higher margination probability in comparison to the smaller ones. Moreover, the distribution of very small particles with a diameter smaller than approximately 250 nm is well represented by the excess volume of RBCs (blood plasma volume). In conclusion, our results suggest that an ellipsoidal shape of carriers with a micron rather than sub-micron size is likely to be favorable for drug delivery.

Acknowledgments

This work has been supported by the DFG Research Unit FOR 1543 “SHENC - Shear Flow Regulation in Hemostasis”. Dmitry A. Fedosov acknowledges funding by the Alexander von Humboldt Foundation. Kathrin Müller acknowledges support by the International Helmholtz Research School of Biophysics and Soft Matter (IHRS BioSoft). We also gratefully acknowledge a CPU time grant by the Jülich Su-

percomputing Center.

References

Abkarian, M., Lartigue, C., Viallat, A., 2002. Tank treading and unbinding of deformable vesicles in shear flow: determination of the lift force. Phys. Rev. Lett. 88, 068103.

Bagge, U., Karlsson, R., 1980. Maintenance of white blood cell margination at the passage through small venular junctions. Microvasc. Res. 20, 92–95.

Blanco, E., Hsiao, A., Mann, A. P., Landry, M. G., Meric-Bernstam, F., Ferrari, M., 2011. Nanomedicine in cancer therapy: innovative trends and prospects. Cancer Sci. 102, 1247–1252.

Cantat, I., Misbah, C., 1999. Lift force and dynamical unbinding of adhering vesicles under shear flow. Phys. Rev. Lett. 83, 880–883.

Champion, J. A., Mitragotri, S., 2006. Role of target geometry in phagocytosis. Proc. Natl. Acad. Sci. USA 103, 4930–4934.

Crowl, L., Fogelson, A. L., 2011. Analysis of mechanisms for platelet near-wall excess under arterial blood flow conditions. J. Fluid Mech. 676, 348–375.

Dasgupta, S., Auth, T., Gompper, G., 2013. Wrapping of ellipsoidal nano-particles by fluid membranes. Soft Matter 9, 5473–5482.

Davis, M. E., Chen, Z. G., Shin, D. M., 2008. Nanoparticle therapeutics: an emerging treatment modality for cancer. Nat. Rev. Drug Discov. 7, 771–782.

De Jong, W. H., Hagens, W. I., Krystek, P., Burger, M. C., Sips, A. J. A. M., Geertsma, R. E., 2008. Particle size-dependent organ distribution of gold nanoparticles after intravenous administration. Biomaterials 29, 1912–1919.

Decuzzi, P., Ferrari, M., 2006. The adhesive strength of non-spherical particles mediated by specific interactions. Biomaterials 27, 5307–5314.

Decuzzi, P., Godin, B., Tanaka, T., Lee, S.-Y., Chiappini, C., Liu, X., Ferrari, M., 2010. Size and shape effects in the biodistribution of intravascularly injected particles. J. Control. Release 141, 320–327.

Duncan, R., 2006. Polymer conjugates as anticancer nanomedicines. Nat. Rev. Cancer 6, 688–701.

Eckstein, E. C., Tilles, A. W., Millero III, F. J., 1988. Conditions for the occurrence of large near-wall excesses of small particles during blood flow. Microvasc. Res. 36, 31–39.

Español, P., Warren, P., 1995. Statistical mechanics of dissipative particle dynamics. Europhys. Lett. 30, 191–196.

Fedosov, D. A., Dao, M., Karniadakis, G. E., Suresh, S., 2014a. Computational biorheology of human blood flow in health and disease. Ann. Biomed. Eng. 42, 368–387.

Fedosov, D. A., Fornleitner, J., Gompper, G., 2012. Margination of white blood cells in microcapillary flow. Phys. Rev. Lett. 108, 028104.

Fedosov, D. A., Gompper, G., 2014. White blood cell margination in microcirculation. Soft Matter 10, 2961–2970.

Fedosov, D. A., Karniadakis, G. E., 2009. Triple-decker: Interfacing atomistic-mesoscopic-continuum flow regimes. J. Comp. Phys. 228, 1157–1171.

Fedosov, D. A., Noguchi, H., Gompper, G., 2014b. Multiscale modeling of blood flow: from single cells to blood rheology. Biomech. Model. Mechanobiol. 13, 239–258.

Ferrari, M., 2005. Cancer nanotechnology: opportunities and challenges. Nat. Rev. Cancer 5, 161–171.

Freund, J. B., 2014. Numerical simulation of flowing blood cells. Annu. Rev. Fluid Mech. 46, 67–95.

Gentile, F., Chiappini, C., Fine, D., Bhavane, R. C., Peluccio, M. S., Cheng, M. M.-C., Liu, X., Ferrari, M., Decuzzi, P., 2008. The effect of shape on the margination dynamics of non-neutrally buoyant particles in two-dimensional shear flows. J. Biomech. 41, 2312–2318.

Goldsmith, H. L., Cokelet, G. R., Gaehtgens, P., 1989. Robin Fahraeus: evolution of his concepts in cardiovascular physiology. Am. J. Physiol. 257, H1005–H1015.

Goldsmith, H. L., Spain, S., 1984. Margination of leukocytes in blood flow through small tubes. Microvasc. Res. 27, 204–222.

Hoogerbrugge, P. J., Koelman, J. M. V. A., 1992. Simulating microscopic hydrodynamic phenomena with dissipative particle dynamics. Europhys. Lett. 19, 155–160.

Huang, R. B., Mocherla, S., Heslinga, M. J., Charoenphol, P., Eniola-Adefeso, O., 2010. Dynamic and cellular interactions of nanoparticles in vascular-targeted drug delivery (review). Mol. Membr. Biol. 27, 312–327.

Jain, R. K., 1988. Determinants of tumor blood flow: a review. Cancer Res. 48, 2641–2658.

Jain, R. K., 1989. Delivery of novel therapeutic agents in tumors: physiological barriers and strategies. J. Natl. Cancer Inst. 81, 570–576.

Jain, R. K., Stylianopoulos, T., 2010. Delivering nanomedicine to solid tumors. Nat. Rev. Clin. Oncol. 7, 653–664.

Kim, S., Kong, R. L., Popel, A. S., Intaglietta, M., Johnson, P. C., 2007. Temporal and spatial variations of cell-free layer width in arterioles. Am. J. Physiol. 293, H1526–H1535.

Kumar, A., Graham, M. D., 2012. Mechanism of margination in confined flows of blood and other multicomponent suspensions. Phys. Rev. Lett. 109, 108102.

Maeda, N., Suzuki, Y., Tanaka, J., Tateishi, N., 1996. Erythrocyte flow and elasticity of microvessels evaluated by marginal cell-free layer and flow resistance. Am. J. Physiol. 271, H2454–H2461.

Messlinger, S., Schmidt, B., Noguchi, H., Gompper, G., 2009. Dynamical regimes and hydrodynamic lift of viscous vesicles under shear. Phys. Rev. E 80, 011901.

Müller, K., Fedosov, D. A., Gompper, G., 2014. Margination of micro- and nano-particles in blood flow and its effect on drug delivery. Sci. Rep. 4, 4871.

Popel, A. S., Johnson, P. C., 2005. Microcirculation and hemorheology. Annu. Rev. Fluid Mech. 37, 43–69.

Pries, A. R., Secomb, T. W., Gaehtgens, P., 1995. Structure and hemodynamics of microvascular networks: heterogeneity and correlations. Am. J. Physiol. 269, H1713–H1722.

Reasor Jr, D. A., Mehrabadi, M., Ku, D. N., Aidun, C. K., 2013. Determination of critical parameters in platelet margination. Ann. Biomed. Eng. 41, 238–249.

Rolland, J. P., Maynor, B. W., Euliss, L. E., Exner, A. E., Denison, G. M., DeSimone, J. M., 2005. Direct fabrication and harvesting of monodisperse, shape-specific nanobiomaterials. J. Am. Chem. Soc. 127, 10096–10100.

Sanhai, W. R., Sakamoto, J. H., Canady, R., Ferrari, M., 2008. Seven challenges for nanomedicine. Nat. Nanotechnol. 3, 242–244.

Sevick, E. M., Jain, R. K., 1989. Viscous resistance to blood flow in solid tumors: effect of hematocrit on intratumor blood viscosity. Cancer Res. 49, 3513–3519.

Slack, J. D., Kanke, M., Simmons, G. H., DeLuca, P. P., 1981. Acute hemodynamic effects and blood pool kinetics of polystyrene microspheres following intravenous administration. J. Pharm. Sci. 70, 660–664.

Tangelder, G. J., Teirlinck, H. C., Slaaf, D. W., Reneman, R. S., 1985. Distribution of blood platelets flowing in arterioles. Am. J. Physiol. 248, H318–H323.

Tilles, A. W., Eckstein, E. C., 1987. The near-wall excess of platelet-sized particles in blood flow: its dependence on hematocrit and wall shear rate. Microvasc. Res. 33, 211–223.

Woldhuis, B., Tangelder, G. J., Slaaf, D. W., Reneman, R. S., 1992. Concentration profile of blood platelets differs in arterioles and venules. Am. J. Physiol. 262, H1217–H1223.

Yuan, F., Salehi, H. A., Boucher, Y., Vasthare, U. S., Tuma, R. F., Jain, R. K., 1994. Vascular permeability and microcirculation of gliomas and mammary carcinomas transplanted in rat and mouse cranial windows. Cancer Res. 54, 4564–4568.

Zhao, H., Shaqfeh, E. S. G., 2011. Shear-induced platelet margination in a microchannel. Phys. Rev. E 83, 061924.